1521-0111/91/2/87–99$25.00
MOLECULAR PHARMACOLOGY
Copyright © 2016 by The American Society for Pharmacology and Experimental Therapeutics
http://dx.doi.org/10.1124/mol.116.106153
Mol Pharmacol 91:87–99, February 2017

Isoform-Specific Biased Agonism of Histamine H_3 Receptor Agonists[S]

Darren M. Riddy,[1] Anna E. Cook,[1] Natalie A. Diepenhorst, Sanja Bosnyak, Ryan Brady, Clotilde Mannoury la Cour, Elisabeth Mocaer, Roger J. Summers, William N. Charman, Patrick M. Sexton, Arthur Christopoulos, and Christopher J. Langmead

Drug Discovery Biology, Monash Institute of Pharmaceutical Sciences, Monash University, Parkville, Victoria, Australia (D.M.R., A.E.C., N.A.D., S.B., R.B., R.J.S., W.N.C., P.M.S., A.C., C.J.L.); and Institut de Recherches Internationales Servier, Suresnes, France (C.M.C., E.M.)

Received July 17, 2016; accepted November 17, 2016

ABSTRACT

The human histamine H_3 receptor (hH_3R) is subject to extensive gene splicing that gives rise to a large number of functional and nonfunctional isoforms. Despite the general acceptance that G protein–coupled receptors can adopt different ligand-induced conformations that give rise to biased signaling, this has not been studied for the H_3R; further, it is unknown whether splice variants of the same receptor engender the same or differential biased signaling. Herein, we profiled the pharmacology of histamine receptor agonists at the two most abundant hH_3R splice variants (hH_3R_{445} and hH_3R_{365}) across seven signaling endpoints. Both isoforms engender biased signaling, notably for 4-[3-(benzyloxy)propyl]-1*H*-imidazole (proxyfan) [e.g., strong bias toward phosphorylation of glycogen synthase kinase 3β (GSK3β) via the full-length receptor] and its congener 3-(1H-imidazol-4-yl)propyl-(4-iodophenyl)-methyl ether (iodoproxyfan), which are strongly consistent with the former's designation as a "protean" agonist. The 80 amino acid IL3 deleted isoform hH_3R_{365} is more permissive in its signaling than hH_3R_{445}: 2-(1*H*-imidazol-5-yl)ethyl imidothiocarbamate (imetit), proxyfan, and iodoproxyfan were all markedly biased away from calcium signaling, and principal component analysis of the full data set revealed divergent profiles for all five agonists. However, most interesting was the identification of differential biased signaling between the two isoforms. Strikingly, hH_3R_{365} was completely unable to stimulate GSK3β phosphorylation, an endpoint robustly activated by the full-length receptor. To the best of our knowledge, this is the first quantitative example of differential biased signaling via isoforms of the same G protein–coupled receptor that are simultaneously expressed in vivo and gives rise to the possibility of selective pharmacological targeting of individual receptor splice variants.

Introduction

It is now generally accepted that G protein–coupled receptors (GPCRs) can be stabilized into different receptor conformations by ligands to engender signaling bias toward some pathways to the relative exclusion of others (Kenakin, 2011; Kenakin and Christopoulos, 2013). Bias has been identified as a universal paradigm across family A, B, and C GPCRs, exemplified, for instance, at the β_2-adrenergic receptor (Liu et al., 2012), parathyroid hormone-1 receptor (Gesty-Palmer et al., 2009), and glucagon-like peptide-1 receptor (Koole et al., 2013), respectively. Biased agonism is now being exploited to develop compounds that preferentially target therapeutically relevant signaling pathways, and away from undesired pathways, thus limiting on-target-mediated side effects (Nijmeijer et al., 2013; Valant et al., 2014).

The histamine H_3 receptor (H_3R) is a GPCR that is widely expressed in human brain with high levels localized to areas associated with cognition, such as the striatum, cerebral cortex, and hippocampus (Pillot et al., 2002). It has been implicated in various pathologies, including Alzheimer's disease, schizophrenia, dementia, Parkinson's disease, depression, and mood disorders (Barbier et al., 2007; Esbenshade et al., 2008; Bitner et al., 2011; Bhowmik et al., 2012; Scott Bitner, 2012), in part due to its function as an auto- and heteroreceptor, controlling the release of various neurotransmitters, including histamine, acetylcholine, dopamine, noradrenaline, GABA, and glutamate (Gbahou et al.,

A.E.C. is a Senior Principal Research Fellow, and P.M.S. is a Principal Research Fellow of the National Health and Medical Research Council of Australia.

[1]D.M.R. and A.E.C. contributed equally to this manuscript.

dx.doi.org/10.1124/mol.116.106153.

[S] This article has supplemental material available at molpharm.aspetjournals.org.

ABBREVIATIONS: A23187, 5-(methylamino)-2-({(2*R*,3*R*,6*S*,8*S*,9*R*,11*R*)-3,9,11-trimethyl-8-[(1*S*)-1-methyl-2-oxo-2-(1*H*-pyrrol-2-yl)ethyl]-1,7-dioxaspiro[5.5]undec-2-yl}methyl)-1,3-benzoxazole-4-carboxylic acid; ABT-239, 4-(2-{2-[(2*R*)-2-Methylpyrrolidin-1-yl]ethyl}-benzofuran-5-yl)benzonitrile; ANOVA, analysis of variance; BSA, bovine serum albumin; $[Ca^{2+}]_i$, intracellular calcium-mobilization assay; DMEM, Dulbecco's modified Eagle's medium; ERK, extracellular signal-regulated kinase; GPCR, G protein–coupled receptor; GSK-189254, 6-[(3-cyclobutyl-1,2,4,5-tetrahydro-3-benzazepin-7-yl)oxy]-*N*-methylpyridine-3-carboxamide; GSK3β, glycogen synthase kinase 3β; GTPγ^{35}S, [^{35}S]guanosine 5′-(γ-thio)triphosphate; H_3R, histamine H_3 receptor; hH_3R, human histamine H_3 receptor; imetit, 2-(1*H*-imidazol-5-yl)ethyl imidothiocarbamate; iodoproxyfan, 3-(1H-imidazol-4-yl)propyl-(4-iodophenyl)-methyl ether; JNJ-5207852, 1-{3-[4-(Piperidin-1-ylmethyl)phenoxy]propyl}piperidine; NαMH, *N*-α-methylhistamine dihydrochloride; PBS, phosphate-buffered saline; PC, principal component; PCA, principal component analysis; pERK, phosphorylated ERK; PLA_2, phospholipase; proxyfan, 4-[3-(benzyloxy)propyl]-1*H*-imidazole; RαMH, (R)(−)-α-methylhistamine dihydrochloride; TM, transmembrane.

2012). The receptor has also been associated with non–central nervous system conditions, such as multiple sclerosis, obesity, and cancer (Berlin et al., 2011).

Due to the localization and function of H_3R, a number of selective H_3R agonists and antagonists have been developed, including 2-(1*H*-imidazol-5-yl)ethyl imidothiocarbamate (imetit), 4-[3-(benzyloxy)propyl]-1*H*-imidazole (proxyfan), thioperamide, ciproxifan, 4-(2-{2-[(2*R*)-2-Methylpyrrolidin-1-yl]ethyl}-benzofuran-5-yl)benzonitrile (ABT-239), 6-[(3-cyclobutyl-1,2,4,5-tetrahydro-3-benzazepin-7-yl)oxy]-*N*-methylpyridine-3-carboxamide (GSK-189254), 1-{3-[4-(Piperidin-1-ylmethyl)phenoxy]propyl}piperidine (JNJ-5207852), and pitolisant (Barbier et al., 2004; Ligneau et al., 2007; Medhurst et al., 2007; Tiligada et al., 2009; Giannoni et al., 2010; Schwartz, 2011). Two H_3R ligands, proxyfan and cipralisant, were initially identified as inverse agonists, but later studies suggested that their pharmacology is more complex (Gbahou et al., 2003; Krueger et al., 2005). Explanations for their apparent "protean" agonism include biased agonism, differential sensitivity to the stoichiometry and type of available G proteins expressed in the cell background, and/or differences in the level of constitutive activity present in the assay system (Gbahou et al., 2003; Krueger et al., 2005).

Moreover, and unlike other histamine receptor subtypes, the H_3R is subject to extensive splicing, yielding a large number of functionally active isoforms (Leurs et al., 2005). Of these, the full-length isoform, human H_3R_{445} (hH_3R_{445}), and the hH_3R_{365} version are the most highly expressed within the human brain. Both isoforms display distinct localization profiles, with hH_3R_{445} showing higher expression in the caudate, corpus callosum, and spinal cord, and hH_3R_{365} being predominant in several areas, including the hypothalamus and cerebellum (Bongers et al., 2007). Interestingly, the 80 amino acid truncation comprises the C-terminal region of IL3 of the full-length receptor, implying that it could mediate differential coupling to intracellular effectors (Huang and Tesmer, 2011), a fact consistent with prior, sometimes conflicting, reports of the overall functionality of hH_3R_{365} (Cogé et al., 2001; Wellendorph et al., 2002; Esbenshade et al., 2006; Arrang et al., 2007; Bongers et al., 2007).

Surprisingly, given the extensive number of probes and signaling pathways reported for the H_3R, there has been no systematic analysis of its ability to engender biased agonism, nor of the impact of alternative splicing on such bias. Therefore, the aim of the current study was to perform a comparative analysis of signaling to various pathways between the key hH_3R_{445} and hH_3R_{365} isoforms, thus focusing not only on "ligand-directed" biased agonism, but also on the potential for "isoform" bias. Strikingly, we identified marked differences in the signaling profile of the two receptor isoforms and, notably, clear divergence in the ligand bias profile between the isoforms. Although previous studies have shown that naturally occurring mutations of the calcium-sensing receptor can give rise to differential signaling compared with the wild-type receptor (Leach et al., 2015), and a very recent paper described splice variant selectivity for the CXCR3 (Berchiche and Sakmar, 2016), to our knowledge, this is the first quantitative assessment of differential agonist bias at isoforms of the same receptor that are simultaneously expressed in vivo. This discovery could underlie some of the complex pharmacology observed for H_3R ligands as well as impacting other therapeutic GPCR targets where multiple receptor isoforms are known to exist.

Materials and Methods

Cell Line Generation and Culture. Stably expressed, tetracycline-inducible, Flp-In-CHO-TREx H_3R cell lines were generated as previously described by Ward et al. (2011). Clones were functionally screened for high expression as determined by the efficacy of imetit in 0.5 and 1 μg/ml tetracycline-treated cells in the inhibition of cAMP accumulation assay. Cell lines were maintained in Dulbecco's modified Eagle's medium (DMEM):Ham's F-12 (1:1) supplemented with 16 mM HEPES, 5 μg/ml blasticidin, 300 μg/ml hygromycin B, and 10% tetracycline-free fetal bovine serum at 37°C/5% CO_2.

Membrane Preparation. Cells were grown to 80–90% confluence in 500 cm^2 cell-culture trays at 37°C/5% CO_2. All subsequent steps were conducted at 4°C to avoid receptor degradation. The cell-culture medium was removed, and ice-cold buffer [10 ml per tray; 10 mM HEPES, 0.9% (w/v) NaCl, 0.2% (w/v) EDTA, pH 7.4] was added to the cells. The cells were scraped from the trays into a 50-ml Corning tube (Corning, NY) and centrifuged at 250 × *g* for 5 minutes. The supernatant fraction was aspirated, and 10 ml per 500-cm^2 tray of wash buffer (10 mM HEPES, 10 mM EDTA, pH 7.4) was added to the pellet that was homogenized using an electrical homogenizer [Werker, ultraturrax, position 6, 4 5-second bursts (Sigma Aldrich, Castle Hill, Australia)] and centrifuged at 48,000 × *g* at 4°C (Beckman Avanti J-251 Ultracentrifuge; Beckman Coulter, High Wycombe, UK) for 30 minutes. The supernatant was discarded and the pellet rehomogenized in wash buffer and centrifuged as described earlier. The final pellet was suspended in ice-cold assay buffer (10 mM HEPES, 0.1 mM EDTA, pH 7.4) at a concentration of 1–2 mg/ml. Protein concentration was determined by a bicinchoninic acid assay, using bovine serum albumin (BSA) as a standard and aliquots maintained at −80°C until required.

[^{3}H]*N*-α-Methyl Histamine Binding. All radioligand experiments were conducted in 10-ml tubes, in assay binding buffer (50 mM Tris-HCL, 5 mM EDTA, pH 7.7), and at 25°C. In all cases, nonspecific binding was determined in the presence of 10 μM ABT-239. After 1-hour incubation, bound and free [^{3}H] *N*-α-methylhistamine dihydrochloride ($N\alpha$MH) were separated by rapid vacuum filtration using a FilterMate Cell Harvester (Perkin Elmer, Melbourne, Australia) onto 96-well GF/B filter mats presoaked with 0.3% polyethylenimine and rapidly washed three times with ice cold wash buffer (50 mM Tris-HCL, 5 mM EDTA, pH 7.7). After drying (>1 hour), filter mats were separated and placed into scintillation vials. To these, 2 ml of Ultima Gold (PerkinElmer) was added, and radioactivity was quantified using liquid scintillation spectrometry (LS 6500 scintillation counter; (Beckman Coulter). Aliquots of [^{3}H]$N\alpha$MH were also quantified accurately to determine how much radioactivity was added to each well. In all experiments, total binding never exceeded more than 10% of that added, limiting complications associated with depletion of the free radioligand concentration.

AlphaScreen SureFire Assays: Inhibition of cAMP Accumulation, Extracellular Signal-Related Kinase 1/2 Phosphorylation, and Glycogen Synthase Kinase 3β pSer9. The inhibition of cAMP accumulation and activation of phosphorylated extracellular signal-related kinase 1/2 (pERK1/2) and glycogen synthase kinase 3β (GSK3β) was measured using AlphaScreen SureFire assay kits (Perkin Elmer, Waltham, MA). Cells were seeded into transparent 96-well plates at 40,000 cells per well in the presence of 1 μg/ml tetracycline and incubated overnight at 37°C/5% CO_2. For the cAMP assay, cells were washed twice with phosphate-buffered saline (PBS) and incubated in stimulation buffer [phenol red–free DMEM (Life Technologies, Melbourne, Australia), 1% BSA, and 1 mM 3-isobutyl-1-methylxanthine] at 37°C/5% CO_2 for 1 hour. For determination of agonist-stimulated concentration-response curves, cells were stimulated with compounds of interest for 10 minutes at 37°C/5% CO_2 prior to addition of 3.16 μM forskolin and incubation at 37°C/5% CO_2 for a further 20 minutes. Media were removed and reactions terminated by addition of 50 μl/well ice-cold 100% ethanol. Cells were incubated at 22°C with shaking for 5 minutes prior to removal

of ethanol by evaporation. To the plate, 100 μl/well lysis buffer (0.1% BSA, 5 mM HEPES, 0.3% Tween) was added followed by shaking for 5 minutes at 22°C. Fetal bovine serum was used as a positive control for the pERK1/2 and GSK3β assays. Compounds were profiled in the pERK1/2 assay using the time to peak as the agonist exposure time (generally 3–4 minutes). These responses were terminated by the removal of drugs and addition of either 100 μl (pERK1/2) or 25 μl (GSK3β) SureFire lysis buffer, and plates were agitated on a plate shaker for 5 minutes. To determine agonist activity, a volume of 5 μl (cAMP and pERK1/2) or 4 μl (GSK3β) of cell lysate was added to a white ProxiPlate (Perkin Elmer), followed by 10 μl (cAMP), 8 μl (pERK1/2), or 5 μl (GSK3β) of 100:600:3:3 (v/v/v/v) mixture of SureFire activation buffer/SureFire reaction buffer/AlphaScreen donor/acceptor beads. All plates were secured with a top seal. cAMP plates were incubated at 22°C overnight, pERK1/2 plates were incubated at 37°C/5% CO_2 for 1 hour, and the GSK3β plates were incubated at 22°C for 2 hours. All plates were incubated in the dark and fluorescence was measured using a Fusion-Alpha or Envision microplate reader (PerkinElmer, Waltham, MA) using standard AlphaScreen settings.

Intracellular Calcium-Mobilization Assays. Assays were performed in isotonic buffer [150 mM NaCl, 2.6 mM KCl, 2.2 mM $CaCl_2$, 1.18 mM $MgCl_2$, 10 mM D-glucose, 10 mM HEPES, 4 mM probenecid, and 0.5% (w/v) BSA, pH 7.4]. Assay buffer was prepared as a (10×) stock (without probenecid or BSA), sterile filtered, and stored at 4°C until required. A (1×) stock (500 ml) of assay buffer was prepared by adding 50 ml of 10× stock and 5 ml of 400 mM probenecid (dissolved in 1 M NaOH) to 440 ml H_20, and pH was adjusted to 7.4, before making up the final volume of 500 ml. BSA [0.5% (w/v)] was added and (1×) assay buffer stored at 4°C for up to 2 weeks.

Cells were seeded into 96-well plates in growth medium at a density of 40,000 cells/well and treated with 1 μg/ml final tetracycline. The following day, plates containing a confluent monolayer of cells were washed twice with 100 μl of assay buffer before being loaded with 100 μl of assay buffer containing 0.9 μM Fluo-4-AM (Sigma-Aldrich, Castle Hill, Australia). After 1-hour incubation at 37°C/5% CO_2, Fluo-4-AM–containing buffer was removed, and wells were washed twice with 100 μl of assay buffer before being loaded with 180 μl of assay buffer. After 20 minutes, compounds were added on a Flexstation microplate reader (Molecular Devices, Sunnyvale, CA). Peak fluorescence was detected using 485-nm excitation and 525-nm emission filters. Data were normalized to the response to 100 μM ATP.

[^{35}S]Guanosine 5′-(γ-thio)triphosphate Binding. Compounds were prepared at 100× final concentration in 100% dimethylsulfoxide, and 2.5 μl was added to a 96-well assay plate. To each well, 200 μl of assay buffer, with 0.1% BSA and 30 μg/ml saponin added fresh on the day of experimentation, containing 50 μg/ml membranes, and 3.7 μM guanosine 5′-diphosphate sodium salt (GDP), was incubated at room temperature with gentle agitation for 30 minutes, allowing equilibrium to be reached. Following this, 50 μl of [^{35}S]guanosine 5′-(γ-thio)triphosphate (GTPγ^{35}S) at a final concentration of 300 pM was added to each well and incubated at 22°C with gentle agitation for 40 minutes. Bound and free GTPγ^{35}S were separated by rapid vacuum filtration using a FilterMate Cell Harvester (PerkinElmer) onto 96-well GF/C filter plates and rapidly washed three times with ice-cold wash buffer (50 mM Tris-HCl, 10 mM $MgCl_2$, 100 mM NaCl, pH 7.6). After drying (>4 hours), 40 μl of MicroScint 20 (PerkinElmer) was added to each well, and radioactivity was quantified using single photon counting on a MicroBeta^2 microplate scintillation counter (PerkinElmer).

[^{3}H]Arachidonic Acid Release: Direct Measurement of Phospholipase Activation. Cells were seeded into 96-well plates at a density of 40,000 cells per well, and receptor expression was induced using 1 μg/ml tetracycline overnight at 37°C/5% CO_2. The following day, cells were washed with PBS and incubated with 0.25 μCi/ml [^{3}H]arachidonic acid in 1:1 DMEM:Ham's F12 containing 0.2% BSA for 2 hours at 37°C/5% CO_2. A time course was initially performed to determine the time at which [^{3}H]arachidonic acid release peaked using 2 μM 5-(methylamino)-2-({(2*R*,3*R*,6*S*,8*S*,9*R*,11*R*)-3,9,11-trimethyl-8-[(1*S*)-1-methyl-2-oxo-2-(1*H*-pyrrol-2-yl)ethyl]-1,7-dioxaspiro[5.5]undec-2-yl}methyl)-1,3-benzoxazole-4-carboxylic acid (A23187) a Ca^{2+} ionophore, and 10 or 100 μM agonist. Following incubation, cells were washed and incubated for 10 minutes with agonists in 1:1 DMEM:Ham's F12 medium. After 10 minutes, 2 μM A23187 was added, and cells were incubated for a further 20 minutes. [^{3}H]Arachidonic acid release was determined by liquid scintillation counting where, following incubation time, supernatant from each well was transferred to a new 96-well white Isoplate, and IRGA-SAFE PLUS (Perkin Elmer) scintillant was added. Plates were left for 30 minutes at room temperature and read on a MicroBeta^2 microplate scintillation counter (PerkinElmer).

Label-Free Technology (Cell Impedance). Experiments were conducted on an RTCA SP xCELLigence instrument (ACEA Biosciences, San Diego, CA) maintained at 37°C/5% CO_2. In brief, a blank read of 100 μl/well of medium was taken. Cells were seeded onto a 96-well E-plate at 20,000 cells/well in the presence of 1 μg/ml tetracycline and allowed to settle for 30 minutes before being replaced in the machine and monitored every 2 minutes and then hourly overnight. Cells were washed with 100 μl/well PBS, and 180 μl/well serum-free medium was added. Cells were then monitored every 15 seconds for 1 hour upon the addition of agonists at varying concentrations. Calculating the area under the cell impedance curves using the RTCA software 1.2 (Roche Diagnostics, Melbourne, Australia) generated agonist concentration-response curves using medium-only wells as baseline.

Compounds and Reagents. All compounds were supplied from Sigma-Aldrich (R-α-methylhistamine, N-α-methylhistamine), Servier (Paris, France; imetit, proxyfan), or synthesized in house [3-(1H-imidazol-4-yl)propyl-(4-iodophenyl)-methyl ether (iodoproxyfan); as described by Stark et al. (1996)]. Radioligands were supplied by PerkinElmer. Cell culture and molecular biology reagents were supplied by Life Technologies (Melbourne, Australia).

Data Analysis. Saturation binding isotherms were analyzed by nonlinear regression according to a hyperbolic, one-site binding model, and individual estimates for total receptor number (B_{max}) and radioligand dissociation constant (K_D) were calculated. The following equation was used, where [A] is the concentration of radioligand:

$$Y = \frac{B_{max}\,[A]}{K_D + [A]} \tag{1}$$

Agonist concentration-response curves were fitted to a sigmoidal three-parameter logistic equation:

$$Y = \text{basal} + \frac{(E_{max} - \text{basal})}{1 + 10^{\cdot}\ (\text{LogEC}_{50} - X)} \tag{2}$$

where Y is the response measured. E_{max} denotes maximal asymptotic response, and basal denotes minimal asymptotic response.

The analysis of the same data sets to quantify biased agonism can be undertaken in a number of ways: transducer ratios [$\text{Log}(\tau/K_A)$], relative activity (RA) ratios [$\Delta\text{Log}(E_{max}/EC_{50})$], and relative potency ratios (ΔpEC_{50}; Kenakin et al., 2012). As not all ligands were full agonists in each system (necessary for simple calculation of relative potency ratios), relative transducer ratios were used as the measure of bias. Data from each individual experiment for each pathway were fitted to an equation that directly estimates $\text{Log}(\tau/K_A)$ and avoids propagation of error associated with fitting individual E_{max} and EC_{50} values using the standard Hill equation:

$$\text{response} = \text{basal} + \frac{(E_m - \text{basal})\left(\frac{\tau}{K_A}\right)^n [A]^n}{[A]^n\left(\frac{\tau}{K_A}\right)^n + \left(1 + \frac{[A]}{K_A}\right)^n} \tag{3}$$

where E_m is the maximal response of the system, basal is the level of response in the absence of agonist, and K_A denotes the equilibrium dissociation constant of the agonist (A); τ/K_A (determined as a logarithm; Christopoulos, 1998) is a composite parameter sufficient to describe

agonism and bias for a given pathway, i.e., stimulus-biased agonism can result from a selective affinity (K_A) of an agonist for a given receptor state(s) and/or a differential coupling efficacy (τ) toward certain pathways, where τ is an index of the signaling efficacy of the agonist (defined as R_T/K_E, where R_T is the total number of receptors, and K_E is the coupling efficiency of each agonist-occupied receptor), and n is the slope of the transducer function.

To remove system bias, $\mathrm{Log}(\tau/K_A)$ values were normalized to the reference agonist (R)(−)-α-methylhistamine dihydrochloride (RαMH). The $\Delta\mathrm{Log}(\tau/K_A)$ value was determined for each ligand, and each pathway was normalized to the RαMH response in the same pathway, according to the following equation:

$$\Delta\mathrm{Log}\left(\frac{\tau}{K_A}\right) = \mathrm{Log}\left(\frac{\tau}{K_A}\right)_{\text{test ligand}} - \mathrm{Log}\left(\frac{\tau}{K_A}\right)_{\mathrm{R}\alpha\mathrm{MH}} \quad (4)$$

To account for the differences in expression (R_T) of hH_3R_{365} and hH_3R_{445}, τ/K_A values for agonists at hH_3R_{365} were normalized using the ratio of maximal binding capacity (B_{max}) values from saturation binding isotherms of [^{3}H]-NαMH (correction factor = 3.36; vide infra, and shown in Supplemental Fig. 1).

The S.E.M. for each $\Delta\mathrm{Log}(\tau/K_A)$ value within the same pathway was calculated according to the following equation:

$$\text{pooled S.E.M.} = \sqrt{(\text{S.E.M.}_{\text{test ligand}})^2 + (\text{S.E.M.}_{\mathrm{R}\alpha\mathrm{MH}})^2} \quad (5)$$

To account for observational bias, the calculated $\Delta\mathrm{Log}(\tau/K_A)$ values were further normalized to the reference pathway, cAMP. The $\Delta\Delta\mathrm{Log}(\tau/K_A)$ value was determined as previously described using the following equation:

$$\Delta\Delta\mathrm{Log}\left(\frac{\tau}{K_A}\right) = \Delta\mathrm{Log}\left(\frac{\tau}{K_A}\right)_{\text{test pathway}} - \Delta\mathrm{Log}\left(\frac{\tau}{K_A}\right)_{\text{cAMP}} \quad (6)$$

The S.E.M. for each $\Delta\Delta\mathrm{Log}(\tau/K_A)$ value was calculated as previously described:

$$\text{pooled S.E.M.} = \sqrt{(\text{S.E.M.}_{\text{test pathway}})^2 + (\text{S.E.M.}_{\text{cAMP}})^2} \quad (7)$$

Differences among $\Delta\mathrm{Log}(\tau/K_A)$ values were compared according to a two-way analysis of variance (ANOVA; with assay and agonist as the two group variables) with multiple planned comparisons using Tukey's test: 1) between pathways for the same agonist and 2) between agonists for the same pathway.

To investigate whether any agonist, at any pathway, was biased toward either of the two receptor isoforms, $\Delta\mathrm{Log}(\tau/K_A)_{445\text{-}365}$ values were calculated using the following equation:

$$\Delta\mathrm{Log}\left(\frac{\tau}{K_A}\right)_{445-365} = \mathrm{Log}\left(\frac{\tau}{K_A}\right)\mathrm{hH_3R_{445}} - \mathrm{Log}\left(\frac{\tau}{K_A}\right)\mathrm{hH_3R_{365}} \quad (8)$$

$\Delta\mathrm{Log}(\tau/K_A)_{445\text{-}365}$ values were compared with a theoretical value of zero (i.e., no isoform bias) using a one-sample t test.

Principal component analysis (PCA) was subsequently applied to the calculated $\Delta\Delta\mathrm{Log}(\tau/K_A)$ bias values obtained in eq. 8 for both isoforms, using singular value decomposition as implemented in the package scikit-learn (scikit-learn.org) (Pedregosa et al., 2011). This analysis is a dimensionality reduction method that uses transformations to project a high-dimensional set of data into a lower-dimensional set of variables, called principal components (PCs) (Thompson et al., 2015). The extracted PC values contain important information from the data, revealing the internal structure in a way that best explains the variance (Wold et al., 1987). PCs are ranked according to the percentage of total variance in the data they explain. PC1 explains the maximal total variance found within the data. The subsequent PC values represent the remaining variation, without being correlated with the preceding components. The script used for the analysis and plotting can be found at https://github.com/thomas-coudrat/pca_analysis.

Results

Expression and Assay Development for Histamine H_3 Receptor Isoforms. To compare the pharmacology of the two most abundantly expressed human histamine H_3 receptor isoforms, CHO-TREx cell lines stably expressing either hH_3R_{365} or hH_3R_{445} were generated. [^{3}H]NαMH saturation binding isotherms were monophasic for both isoforms and revealed that the hH_3R_{445} isoform (B_{max} = 2541 ± 77 fmol/mg protein) was expressed at over 3 times the level of the hH_3R_{365} isoform (B_{max} = 757 ± 52 fmol/mg protein; exact ratio 3.36; Supplemental Fig. 1), with no significant difference in affinity [pK_D values 8.90 ± 0.30 and 8.80 ± 0.90, respectively; grouped data are shown ±S.E.M. (n = 3)].

Concentration-response curves for each of the five histamine receptor agonists (RαMH, imetit, NαMH, proxyfan, and iodoproxyfan; Fig. 1) were generated in functional assays of: 1) inhibition of forskolin-stimulated cAMP accumulation, 2) intracellular calcium-mobilization, 3) ERK1/2 phosphorylation, 4) GTPγ^{35}S binding, 5) phospholipase A_2 (PLA_2) activity ([^{3}H]arachidonic acid release), 6) GSK3β phosphorylation, and 7) cell impedance. Somewhat surprisingly, all agonist-evoked responses at both isoforms were blocked by an overnight treatment with pertussis toxin (10 ng/ml), indicating that all downstream signaling was via $G_{i/o}$ protein coupling (data not shown).

Generally, all five compounds displayed agonist activity in all signaling assays and at both isoforms, with potencies being approximately 10-fold higher at the hH_3R_{445} isoform compared with hH_3R_{365} (Figs. 2 and 3; Supplemental Tables 1 and 2), in part reflecting the higher expression of the former. For hH_3R_{445}, agonists were most potent for the inhibition of cAMP accumulation and GSK3β phosphorylation (Fig. 2; Table 1), with a general rank order of potencies being inhibition of cAMP accumulation = GSK3β > pERK1/2 = PLA_2 = GTPγ^{35}S binding > $[Ca^{2+}]_i$ mobilization > cell impedance (Fig. 2; Supplemental Table 1). At hH_3R_{365}, a similar profile was observed across most assays, although strikingly, this isoform was completely unable to stimulate the phosphorylation of GSK3β, the most sensitive assay for hH_3R_{445} (Fig. 3; Supplemental Table 2). More subtly, the potencies to promote GTPγ^{35}S binding were closer to those obtained in the inhibition of cAMP accumulation assay compared with hH_3R_{445}, the general rank order of potency being inhibition of cAMP accumulation > GTPγ^{35}S binding > PLA_2 = pERK1/2 > $[Ca^{2+}]_i$ mobilization > cell impedance (Fig. 3; Supplemental Table 2).

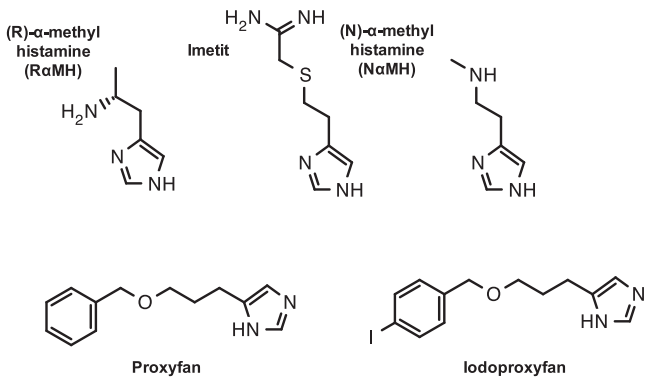

Fig. 1. Structures of hH_3R agonists used for the study.

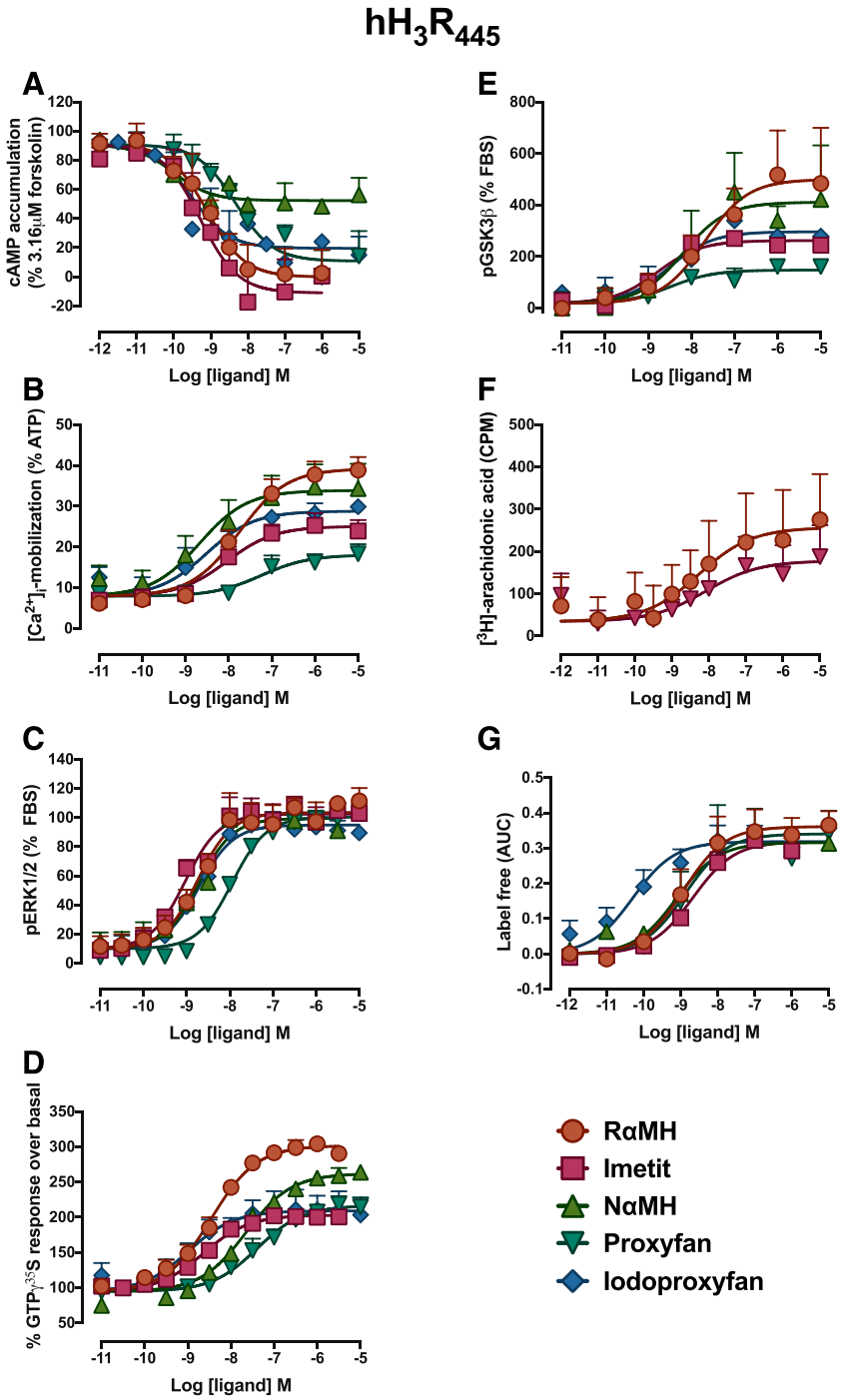

Fig. 2. Concentration-response curves of the five agonists in inhibition of cAMP accumulation (A), $[Ca^{2+}]_i$ mobilization (B), pERK1/2 (C), GTPγ^{35}S binding (D), pGSK3β (E), PLA_2 (F), and cell impedance assays (G) at the hH_3R_{445}. Experiments were performed as described in *Materials and Methods*. The equations as described in the *Data Analysis* section were fitted to the data to estimate EC_{50} and E_{max} values (Supplemental Table 1) or to calculate $\text{Log}\tau/K_A$ values for the agonists (Table 1). Grouped data are shown ±S.E.M. (n = 3–7). AUC, area under the curve; FBS, fetal bovine serum; pGSK3β, phosphorylated GSK3β.

In general, RαMH and NαMH behaved as full agonists in all assays and at both isoforms (with the exception of NαMH in the inhibition of cAMP accumulation assay; Figs. 2 and 3). However, imetit, proxyfan, and iodoproxyfan yielded more variable responses, with different rank orders of activity across assays and partial agonist versus full agonist behaviors (Figs. 2 and 3). Agonist responses at both receptor isoforms were quantitatively assessed using the transducer ratio method (Kenakin et al., 2012) to determine biased agonism both within and between isoforms.

Evaluation of Biased Agonism at the Full-Length Histamine H_3 Receptor. For both isoforms, RαMH was used as the reference agonist to calculate $\Delta\text{Log}(\tau/K_A)$ values (Figs. 4, A and B; 5, A and B; Tables 1 and 2); these values were normalized to the inhibition of cAMP accumulation as the reference pathway to generate $\Delta\Delta\text{Log}(\tau/K_A)$ values (Fig. 5, C and D; Tables 1 and 2). Interestingly, NαMH, a regioisomer of RαMH, displayed no significant biased signaling at hH_3R_{445} (Figs. 4 and 5; Table 1). Imetit followed a similar pattern, although when the data set is normalized to the inhibition of cAMP [i.e., $\Delta\Delta\text{Log}(\tau/K_A)$], it displayed clear bias toward GSK3β (36-fold) and ERK1/2 (12-fold) phosphorylation (Fig. 5C; Table 1).

Perhaps unsurprisingly, proxyfan, the "protean" agonist of the histamine H_3 receptor, displayed a much more varied profile; it was significantly biased away from the inhibition of

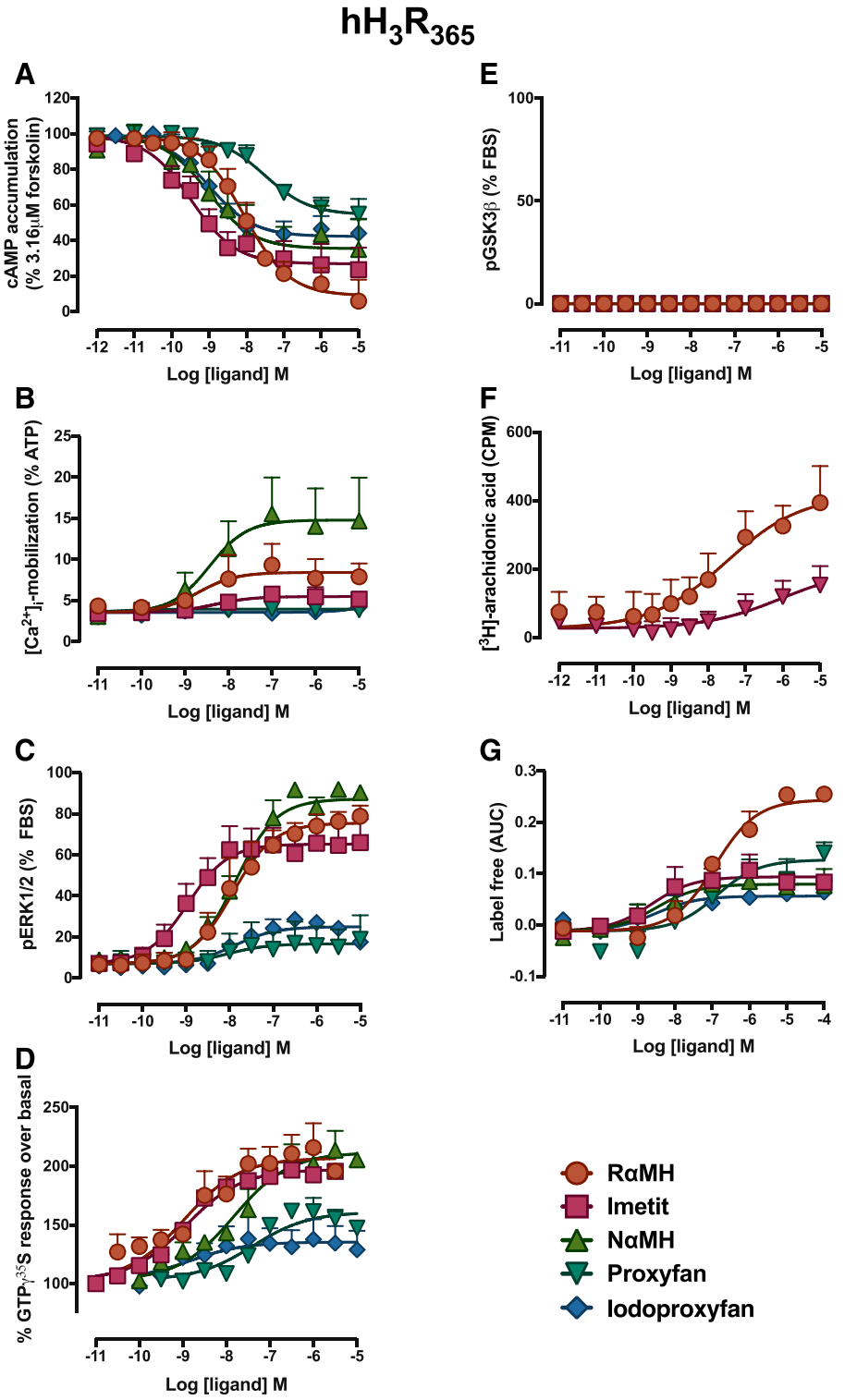

Fig. 3. Concentration-response curves of the five agonists in inhibition of cAMP accumulation (A), $[Ca^{2+}]_i$ mobilization (B), pERK1/2 (C), GTPγ^{35}S binding (D), pGSK3β (E), PLA_2 (F), and cell impedance assays at the hH_3R_{365} (G). Experiments were performed as described in *Materials and Methods*. The equations as described in the *Data Analysis* section were fitted to the data to estimate EC_{50} and E_{max} values (Supplemental Table 2) or to calculate $Log\tau/K_A$ values for the agonists (Table 2). Grouped data are shown ±S.E.M. (n = 3–8). AUC, area under the curve; FBS, fetal bovine serum; pGSK3β, phosphorylated GSK3β.

cAMP, trending in the same direction for calcium mobilization, ERK1/2 phosphorylation, and GTPγ^{35}S binding. Given the relative lack of activity to inhibit cAMP accumulation, when the data were normalized to this pathway, proxyfan displayed marked bias toward GSK3β phosphorylation (260-fold), changes in cellular impedance (28-fold), and ERK1/2 phosphorylation (6.6-fold; Fig. 5C; Table 1). Iodoproxyfan also displayed significant bias toward a change in cell impedance, a response that was itself significantly different from its ability to inhibit forskolin-stimulated cAMP accumulation at the hH_3R_{445} isoform. When normalized to the latter, marked bias toward changes in cellular impedance (150-fold) and GSK3β phosphorylation (33-fold) was evident (Fig. 5C; Table 1).

Evaluation of Biased Agonism at the IL3 Deleted Histamine H_3 Receptor. Our subsequent study sought to determine whether the 80 amino acid deleted receptor, hH_3R_{365},

TABLE 1

Logτ/K_A, ΔLogτ/K_A (normalized to RαMH), and $\Delta\Delta$Logτ/K_A (normalized to cAMP) values for the hH_3R_{445} isoform as determined from the different signaling assays

Data are expressed as the mean ± S.E.M. from a single fit to grouped data of the indicated number (N) of individual experiments, and n is the transducer slope determined from shared analysis. Values in parentheses were used to plot the webs of bias presented in Fig. 5.

Analysis	N	n	RαMH	Imetit	NαMH	Proxyfan	Iodoproxyfan
cAMP							
Logτ/K_A	3–7	0.85 ± 0.18	11.62 ± 0.36	10.98 ± 0.32	12.04 ± 0.28	10.07 ± 0.28	10.98 ± 0.47
ΔLogτ/K_A versus RαMH			0.00 ± 0.46	−0.64 ± 0.45	0.42 ± 0.43	−1.55 ± 0.43	−0.64 ± 0.57
$\Delta\Delta$Logτ/K_A versus cAMP			0.00 ± 0.65 (1.0)	0.00 ± 0.64 (1.0)	0.00 ± 0.61 (1.0)	0.00 ± 0.60 (1.0)	0.00 ± 0.80 (1.0)
$[Ca^{2+}]_i$-mobilization							
Logτ/K_A	4–5	0.79 ± 0.17	9.32 ± 0.17	9.61 ± 0.24	9.54 ± 0.23	8.31 ± 0.21	9.27 ± 0.39
ΔLogτ/K_A versus RαMH			0.00 ± 0.25	0.29 ± 0.29	0.22 ± 0.29	−1.01 ± 0.27	−0.04 ± 0.43
$\Delta\Delta$Logτ/K_A versus cAMP			0.00 ± 0.52 (1.0)	0.93 ± 0.54 (8.5)	−0.20 ± 0.52 (0.6)	0.54 ± 0.51 (3.5)	0.60 ± 0.71 (4.0)
pERK1/2							
Logτ/K_A	3–4	1.10 ± 0.11	10.73 ± 0.16	11.14 ± 0.04	10.63 ± 0.07	10.01 ± 0.10	10.69 ± 0.07
ΔLogτ/K_A versus RαMH			0.00 ± 0.22	0.41 ± 0.16	−0.10 ± 0.17	−0.72 ± 0.18	0.04 ± 0.17
$\Delta\Delta$Logτ/K_A versus cAMP			0.00 ± 0.51 (1.0)	1.05 ± 0.48 (11.1)	−0.52 ± 0.46 (0.3)	0.82 ± 0.46 (6.7)	0.60 ± 0.59 (4.0)
GTPγ^{35}S binding							
Logτ/K_A	3	0.82 ± 0.08	10.65 ± 0.03	10.58 ± 0.04	10.06 ± 0.08	9.44 ± 0.21	10.85 ± 0.07
ΔLogτ/K_A versus RαMH			0.00 ± 0.04	−0.07 ± 0.05	−0.59 ± 0.09	−1.21 ± 0.21	0.21 ± 0.07
$\Delta\Delta$Logτ/K_A versus cAMP			0.00 ± 0.46 (1.0)	0.57 ± 0.46 (3.7)	−1.01 ± 0.44 (0.1)	0.34 ± 0.48 (2.2)	0.85 ± 0.57 (7.0)
pGSK3β							
Logτ/K_A	3	0.87 ± 0.26	10.30 ± 0.18	11.21 ± 0.08	10.67 ± 0.41	11.16 ± 0.72	11.17 ± 0.65
ΔLogτ/K_A versus RαMH			0.00 ± 0.25	0.92 ± 0.19	0.37 ± 0.45	0.86 ± 0.74	0.87 ± 0.67
$\Delta\Delta$Logτ/K_A versus cAMP			0.00 ± 0.52 (1.0)	1.56 ± 0.49 (36.0)	−0.05 ± 0.62 (0.9)	2.41 ± 0.85 (258.8)	1.52 ± 0.88 (32.7)
[^{3}H]arachidonic acid							
Logτ/K_A	3–4	0.60 ± 0.45	10.87 ± 0.51	ND	ND	10.05 ± 0.37	ND
ΔLogτ/K_A versus RαMH			0.00 ± 0.72			−0.82 ± 0.63	
$\Delta\Delta$Logτ/K_A versus cAMP			0.00 ± 0.85 (1.0)			0.73 ± 0.76 (5.3)	
Label free							
Logτ/K_A	3–5	0.77 ± 0.15	8.31 ± 0.37	8.21 ± 0.22	8.51 ± 0.07	8.21 ± 0.39	9.84 ± 0.52
ΔLogτ/K_A versus RαMH			0.00 ± 0.52	−0.10 ± 0.43	0.20 ± 0.37	−0.10 ± 0.54	1.53 ± 0.64
$\Delta\Delta$Logτ/K_A versus cAMP			0.00 ± 0.69 (1.0)	0.54 ± 0.62 (3.5)	−0.22 ± 0.57 (0.6)	1.45 ± 0.68 (28.1)	2.17 ± 0.85 (147.9)

ND, not determined; pGSK3β, phosphorylated pGSK3β.

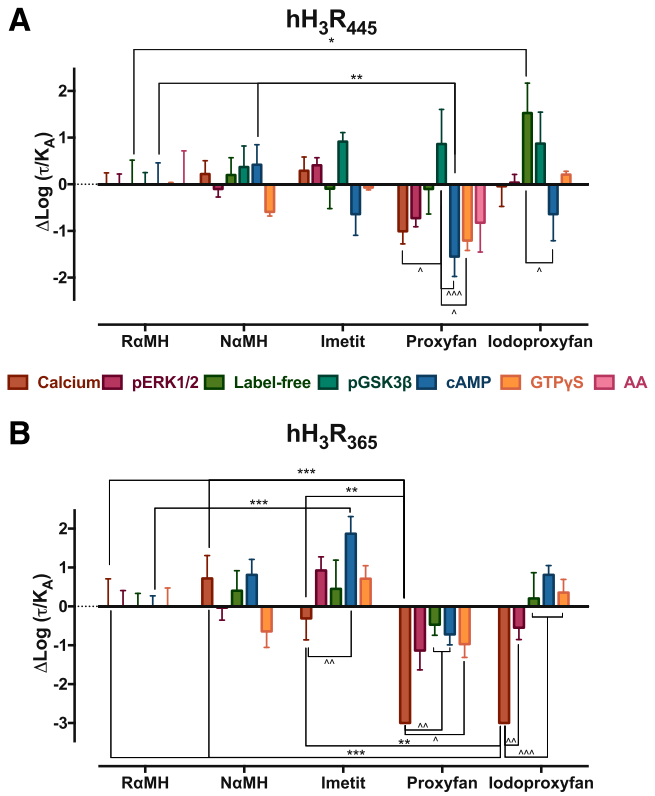

Fig. 4. $\Delta\text{Log}(\tau/K_A)$ values for each agonist in each assay with respect to RαMH for hH_3R_{445} (A) and hH_3R_{365} (B) isoforms. Data represent the mean ± S.E.M. (n = 3–8). For hH_3R_{445}, two-way ANOVA of $\Delta\text{Log}(\tau/K_A)$ values revealed a significant effect of both agonist (P = 0.004) and assay (P = 0.002), but no interaction (P = 0.22). For hH_3R_{365}, there was a highly significant effect of agonists ($P < 0.0001$) and assay ($P < 0.0001$) and a very significant interaction between the two variables (P = 0.0008). For Tukey's planned comparisons testing: $^*P < 0.05$, $^{**}P < 0.01$, and $^{***}P < 0.001$ between agonists for the same assay; $^{\wedge}P < 0.05$, $^{\wedge\wedge}P < 0.01$, and $^{\wedge\wedge\wedge}P < 0.001$ between assays for the same agonist. AA, arachidonic acid (PLA_2); pGSK3β, phosphorylated GSK3β.

could also mediate biased agonism. Overall, this isoform appeared more permissive in its signaling than the full-length receptor (Figs. 4 and 5; Table 2). Two-way ANOVA of resultant $\Delta\text{Log}(\tau/K_A)$ values in Table 2 revealed a highly significant effect of agonists ($P < 0.0001$) and assay ($P < 0.0001$), but also a very significant interaction between the two variables (P = 0.0008), an effect absent at hH_3R_{445} (P = 0.22; Fig. 4).

Although NαMH displayed no substantial differences compared with the reference agonist RαMH, the profiles of imetit, proxyfan, and iodoproxyfan were highly divergent, confirming the presence of significant bias downstream of the receptor (Figs. 4B and 5, B and D; Table 2). Imetit was significantly (74-fold) biased toward the inhibition of cAMP accumulation relative to RαMH. Normalization of the responses to this pathway revealed that imetit was markedly biased *away* from calcium mobilization (0.007-fold), cellular impedance (0.01-fold), GTPγ^{35}S binding (0.07-fold), and ERK1/2 phosphorylation (0.1-fold).

Interestingly, proxyfan and iodoproxyfan were unable to evoke, and hence were highly biased away from, calcium mobilization responses at the hH_3R_{365} isoform, despite robust responses to RαMH, NαMH, and imetit (Fig. 4B; Supplemental Table 2; Table 2). Accordingly, their activity relative to RαMH was fixed to an arbitrary $\Delta\text{Log}(\tau/K_A)$ value of −3.0. This extreme bias away from calcium mobilization for proxyfan and its congener was notable, as it was the only functional endpoint for which either compound displayed bias relative to RαMH [all other pathways, bar pERK1/2 for proxyfan, were significantly different from the fixed $\Delta\text{Log}(\tau/K_A)$ value of −3.0 for both agonists; Fig. 4B]. Even when normalized to cAMP as a reference pathway, only iodoproxyfan exhibited any other biased agonism, being biased away from ERK1/2 phosphorylation (0.04-fold; Figs. 4B and 5, B and D; Table 2).

The Histamine H_3 Receptor Exhibits "Isoform Bias." Although both the full-length and 80 amino acid deleted H_3R mediate biased agonism, it remained to be determined whether the direction and magnitude of the bias were conserved *between* isoforms. Strikingly, none of the agonists stimulated GSK3β phosphorylation via hH_3R_{365}, a pathway readily activated by the hH_3R_{445} isoform, indicating that the hH_3R_{365} isoform is highly biased away from this endpoint (although no quantification was possible due to the lack of activity of any ligand).

Even for pathways activated by both isoforms, visual inspection of the "webs of bias" in Fig. 5 suggests that the pharmacology of the hH_3R_{445} and hH_3R_{365} isoforms is different. To test this assertion, $\text{Log}(\tau/K_A)$ values for each agonist in each assay at hH_3R_{365} were subtracted from the corresponding values at the hH_3R_{445} isoform (Fig. 6). A value that is not significantly different from zero suggests that the agonist is equieffective at both receptor isoforms.

Individual one-sample T-tests for the values reveal a number of significant examples of isoform bias. Proxyfan and iodoproxyfan only promoted calcium mobilization via the hH_3R_{445} isoform, whereas RαMH was approximately 13-fold more effective at inhibiting cAMP levels at this isoform compared with hH_3R_{365}. However, imetit was significantly more efficient at promoting G protein coupling (GTPγ^{35}S binding) at the hH_3R_{365} isoform (Fig. 6). Given the subtle differences in localization and function of the two major isoforms of the H_3 receptor, choice of agonist could influence the observed response(s) and may represent a novel route to selective pharmacology.

To ensure that receptor desensitization or internalization did not markedly influence the bias analysis across the two isoforms, concentration-response curves for each agonist were constructed at varying incubation times using the cAMP assay (data not shown). At the 10-minute time point that we routinely used for agonist incubations, only minimal desensitization was observed for both receptor isoforms and appeared comparable for all agonists tested (percentage response to 10 μM agonist compared with the 2-minute time point, ranging from 76.4 ± 1.8 to 87.6 ± 5.6 and 82.2 ± 6.1 to 92.2 ± 2.3 for the hH_3R_{445} and hH_3R_{365} isoforms, respectively; Supplemental Fig. 2, A and B). In addition, $\Delta\text{Log}\tau/K_A$ values (with reference to RαMH) were calculated and did not significantly change over time (Supplemental Fig. 2, C and D).

Principal Component Analysis. The bias factors $[\Delta\Delta\text{Log}(\tau/K_A)]$ for the two receptor isoforms were then subjected to PCA, a dimensionality reduction method, to reveal values in the data set that contribute variability between ligands. Ligands that display similar behavior cluster together. At hH_3R_{445}, NαMH clustered most closely with RαMH (in PC1) and clearly separated from proxyfan and, to a lesser degree, iodoproxyfan (Fig. 7A). The composite of both PC1 (83%) and PC2 (10%) accounted for 93% of the total variability,

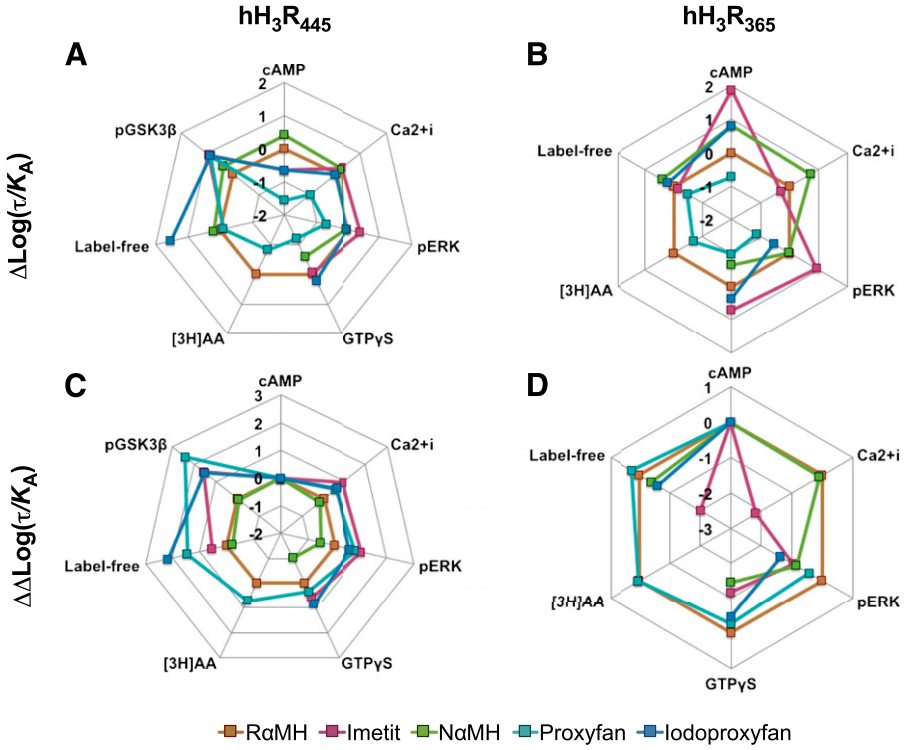

Fig. 5. Webs of bias of agonist-stimulated responses of a range of histamine agonists for hH_3R_{445} (A) and hH_3R_{365} (B) isoforms normalized to the values obtained for the reference agonist RαMH [axes represent $\Delta Log(\tau/K_A)$]. Webs of bias of agonist-stimulated response values at hH_3R_{445} (C) and hH_3R_{365} (D) isoforms normalized to the values obtained for the reference pathway, cAMP [axes represent $\Delta\Delta Log(\tau/K_A)$]. Values used to plot these webs are shown in Tables 1 and 2 in parentheses. AA, arachidonic acid (PLA_2); pGSK3β, phosphorylated GSK3β.

indicating limited variation within this data set. This simple representation reflects what is intuitively visualized in the "web of bias" for hH_3R_{445} (Fig. 5C).

Consistent with the more variable pharmacology and permissive signaling of hH_3R_{365}, there was no evidence of ligand clustering, suggesting that all ligands produce different bias profiles at this isoform, again correlating with their corresponding bias plots (Figs. 5D and 7B). Indeed, comparison of the two principal component analysis plots intuitively reveals the isoform bias that exists between hH_3R_{445} and hH_3R_{365}.

Discussion

Although the histamine H_3 receptor has long been a therapeutic target of considerable interest, its ability to engender biased signaling has not been comprehensively investigated. Herein, we demonstrated not only that can agonists give rise to biased signaling (ligand-directed bias), but also that the two most abundant human H_3R splice variants (hH_3R_{445} and hH_3R_{365}) engender different responses (isoform bias).

The regioisomeric agonists, RαMH and NαMH, display similar pharmacology, with no bias at the hH_3R_{445} isoform. The structurally related agonist, imetit, also had a similar profile, although analysis revealed bias toward phosphorylation of GSK3β and ERK1/2. Strikingly, proxyfan, as well its congener iodoproxyfan, produces clearly divergent signaling at the full-length H_3R with marked bias toward GSK3β phosphorylation and changes in cellular impedance (Figs. 4 and 5). Their distinct profiles, compared with both the histamine analogs as well as each other, are reflected in a PCA of the bias factors (Fig. 7A).

The quantitative confirmation of biased agonism with proxyfan (and iodoproxyfan) helps to explain previous studies that have variously described proxyfan as an inverse agonist, antagonist, partial agonist, or full agonist due to its context-dependent pharmacology (Gbahou et al., 2003; Krueger et al., 2005). This compound's protean agonism has been previously attributed to the degree of constitutive receptor activity present in the assay system being tested (Morisset et al., 2000; Bongers et al., 2007). However, in our studies, constitutive activity was only evident at hH_3R_{445} in the inhibition of cAMP accumulation and GTPγ^{35}S binding assays (data not shown), suggesting that constitutive activity does not appear to influence the bias that proxyfan engenders.

Another aim of this study was to determine the bias profile of the most abundant isoform of the histamine H_3 receptor, hH_3R_{365}. This splice variant was also subject to biased agonism; notably, neither proxyfan nor iodoproxyfan stimulated calcium mobilization via hH_3R_{365}, despite robust responses to NαMH and RαMH (Fig. 3; Table 2). Overall, the profiles of imetit, proxyfan, and iodoproxyfan across the endpoints tested were distinct to NαMH, RαMH, and each other, confirming that this isoform is permissive in its signaling, an assertion supported by the lack of clustering of ligands in the PCA (Fig. 7B) and the highly significant interaction between ligands and assays in the two-way ANOVA of the $\Delta Log(\tau/K_A)$ values for hH_3R_{365} (Fig. 4).

The molecular basis of biased agonism for the hH_3R is unclear. Many prominent examples of biased agonism distinguish between G protein–dependent and G protein–independent signaling (Kenakin and Christopoulos, 2013), but herein, we found that all of the functional responses are sensitive to prior treatment of the cells with pertussis toxin, implying that all of the signaling is downstream of the $G_{i/o}$ family of G proteins. As such, the observed biased agonism may arise from activation of different Gα or G$\beta\gamma$ subunits, as previously demonstrated for the β_3-adrenoceptor (Sato et al., 2007), or variations in drug-receptor kinetics.

TABLE 2

Logτ/K_A, ΔLogτ/K_A (normalized to RαMH), and $\Delta\Delta$Logτ/K_A (normalized to cAMP) values for the hH_3R_{365} isoform as determined from the different signaling assays

Data are corrected for differences in receptor expression as determined by saturation isotherms of [^{3}H]*N*-α-methyl-histamine and are expressed as the mean ± S.E.M. from a single fit to grouped data of the indicated number (N) of individual experiments; *n* is the transducer slope determined from shared analysis. Values in parentheses were used to plot the webs of bias presented in Fig. 5.

Analysis	N	*n*	RαMH	Imetit	NαMH	Proxyfan	Iodoproxyfan
cAMP							
Logτ/K_A	5–8	0.73 ± 0.11	10.52 ± 0.19	12.39 ± 0.40	11.33 ± 0.35	9.80 ± 0.19	11.33 ± 0.14
ΔLogτ/K_A versus RαMH			0.00 ± 0.27	1.87 ± 0.44	0.81 ± 0.40	−0.72 ± 0.27	0.81 ± 0.24
$\Delta\Delta$Logτ/K_A versus cAMP			0.00 ± 0.53 (1.0)	0.00 ± 0.63 (1.0)	0.00 ± 0.58 (1.0)	0.00 ± 0.51 (1.0)	0.00 ± 0.62 (1.0)
$[Ca^{2+}]_i$-mobilization							
Logτ/K_A	3–4	1.00 ± 0.43	9.23 ± 0.50	8.92 ± 0.20	9.95 ± 0.31	NE	NE
ΔLogτ/K_A versus RαMH			0.00 ± 0.71	−0.31 ± 0.54	0.72 ± 0.59	−3.0	−3.0
$\Delta\Delta$Logτ/K_A versus cAMP			0.00 ± 0.84 (1.0)	−2.18 ± 0.70 (0.01)	−0.09 ± 0.73 (0.8)	NA	NA
pERK1/2							
Logτ/K_A	3–5	0.93 ± 0.12	10.29 ± 0.29	11.22 ± 0.19	10.26 ± 0.13	9.16 ± 0.41	9.75 ± 0.10
ΔLogτ/K_A versus RαMH			0.00 ± 0.41	0.93 ± 0.35	−0.03 ± 0.32	−1.14 ± 0.50	−0.55 ± 0.31
$\Delta\Delta$Logτ/K_A versus cAMP			0.00 ± 0.61 (1.0)	−0.94 ± 0.57 (0.1)	−0.84 ± 0.53 (0.1)	−0.42 ± 0.66 (0.4)	−1.36 ± 0.65 (0.04)
GTPγ^{35}S binding							
Logτ/K_A	3	0.68 ± 0.13	10.74 ± 0.33	11.45 ± 0.03	10.10 ± 0.24	9.77 ± 0.06	11.16 ± 0.04
ΔLogτ/K_A versus RαMH			0.00 ± 0.47	0.71 ± 0.34	−0.65 ± 0.41	−0.97 ± 0.34	0.36 ± 0.34
$\Delta\Delta$Logτ/K_A versus cAMP			0.00 ± 0.66 (1.0)	−1.16 ± 0.56 (0.1)	−1.45 ± 0.59 (0.04)	−0.25 ± 0.55 (0.6)	−0.45 ± 0.66 (0.4)
pGSK3β							
Logτ/K_A	3	NE	NE	NE	NE	NE	NE
ΔLogτ/K_A versus RαMH							
$\Delta\Delta$Logτ/K_A versus cAMP							
[^{3}H]arachidonic acid							
Logτ/K_A	4	0.43 ± 0.20	10.73 ± 0.17	ND	ND	9.65 ± 0.40	ND
ΔLogτ/K_A versus RαMH			0.00 ± 0.25			−1.08 ± 0.43	
$\Delta\Delta$Logτ/K_A versus cAMP			0.00 ± 0.52 (1.0)			0.03 ± 0.61 (1.1)	
Label free							
Logτ/K_A	3–4	0.78 ± 0.20	8.21 ± 0.24	8.07 ± 0.53	8.61 ± 0.46	7.74 ± 0.14	8.41 ± 0.62
ΔLogτ/K_A versus RαMH			0.00 ± 0.33	−0.14 ± 0.58	0.40 ± 0.52	−0.47 ± 0.27	0.21 ± 0.66
$\Delta\Delta$Logτ/K_A versus cAMP			0.00 ± 0.57 (1.0)	−2.01 ± 0.74 (0.01)	−0.41 ± 0.67 (0.4)	0.25 ± 0.51 (1.8)	−0.60 ± 0.87 (0.2)

NA, not applicable; ND, not determined; NE, no effect; pGSK3β, phosphorylated pGSK3β.

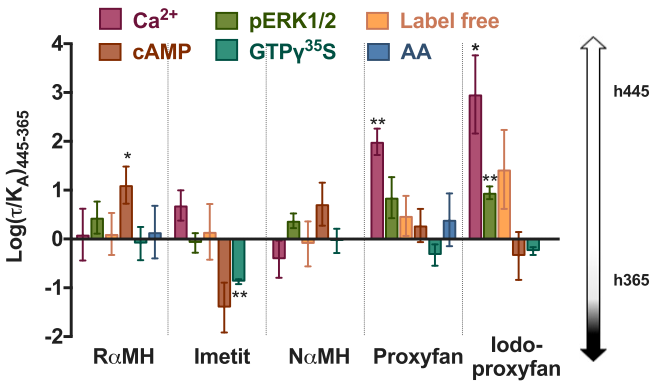

Fig. 6. Comparison of Log(τ/K_A) values for each agonist in each assay between the different isoforms. Values > 0 denote bias toward hH_3R_{445}, whereas values < 0 denote bias toward hH_3R_{365}. Grouped data are shown ±S.E.M. ($n = 3$–8). Statistical significance was deemed by one-sample t test (*$P < 0.05$, **$P < 0.01$ compared with zero, i.e., no isoform bias). AA, arachidonic acid (PLA_2).

The latter is emerging as a key consideration in GPCR discovery, rationalizing in vivo efficacy, drug duration of action, and selectivity (Hoffmann et al., 2015; Riddy et al., 2015; Copeland, 2016). More recent studies have also implicated the kinetics of signaling as a key component of biased agonism (Klein Herenbrink et al., 2016). Given that the assays described herein measure endpoints that range from 15 seconds (calcium mobilization) to 60 minutes (cellular impedance), temporal differences could underlie the observed signaling profiles for proxyfan and iodoproxyfan. Previous studies have shown that intrinsic efficacy of muscarinic M_3 receptor agonists correlates with their dissociation rates; agonists that displayed slow dissociation had higher efficacy in calcium mobilization and GTPγ^{35}S binding assays (Sykes et al., 2009). Therefore, the bias profiles of proxyfan and iodoproxyfan could be due to differential receptor binding kinetics when compared with the simpler histamine analogs, although determination of such properties is beyond the scope of this study. Interestingly, the different lengths of incubation of the signaling assays presented here could explain why the observed bias at the hH_3R_{445} isoform in this study contrasts with that of Schnell et al. (2010), in which the same agonists displayed no bias when assessed by steady-state GTPase activity with various coexpressed G proteins in Sf9 insect cells.

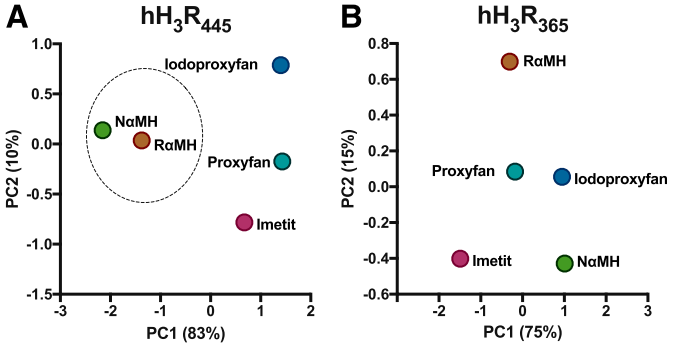

Fig. 7. PCA of the calculated ΔΔLog(τ/K_A) bias factors for hH_3R_{445} (A) and hH_3R_{365} (B) receptor isoforms in response to a range of agonists across the different functional assays, with data being normalized to the values obtained for RαMH and to cAMP as the reference pathway.

In addition to the identification of biased agonism at H_3R splice variants, we then sought to compare the bias profiles of the two isoforms (appropriately corrected for differences in receptor expression). Unexpectedly, there was a striking difference in signaling between the two major splice variants, which we termed "isoform bias." Despite the absence of 80 amino acids in the third intracellular loop in hH_3R_{365} (Leurs et al., 2005; Bongers et al., 2007) and the importance of this region in G protein coupling (O'Dowd et al., 1988), hH_3R_{365} elicits G protein–dependent signaling. Nonetheless, this truncation results in a receptor that robustly couples to some pathways (e.g., inhibition of cAMP accumulation, GTPγ^{35}S binding), as with hH_3R_{445}, but which is completely unable to activate others (GSK3β phosphorylation) and only permissively links to further pathways (e.g., RαMH versus proxyfan in calcium mobilization). This striking isoform bias between the two variants was quantified by calculation of the difference in Log(τ/K_A) values for each agonist at each pathway, and revealed a general preference for imetit to activate pathways downstream of the hH_3R_{365} isoform, with iodoproxyfan and proxyfan favoring the full-length receptor (Fig. 6).

The cause of the differential pharmacology between hH_3R_{445} and hH_3R_{365} isoforms is not clear; previous studies using G protein–coupled inward rectifier potassium channel activation as a surrogate of receptor activation showed that the hH_3R_{365} isoform yielded G protein–coupled inward rectifier potassium channel responses with a 5- to 6-fold increase in deactivation kinetics compared with hH_3R_{445}, implying that agonists may have a slower off-rate than this isoform (Sahlholm et al., 2012). It is also possible that the kinetic rate(s) of GDP/GTP exchange may differ between isoforms (Dror et al., 2015). An alternative explanation could be that the differences arise due to a change in the distances between transmembrane (TM) domains 5 and 6 between isoforms. Using all known inactive GPCR structures, Kruse et al. (2012) demonstrated that the distance between the bases of TM5 and TM6 of G$\alpha_{i/o}$-coupled receptors ranged between 12.5 and 14.5 Å, whereas for Gα_s-coupled receptors, this distance was shorter, ranging from 10 to 12 Å. The distance between TM5 and TM6 for the hH_3R_{365} isoform may be reduced, resulting in a receptor that differentially couples to G protein isoforms, in turn activating different signaling networks.

Irrespective of mechanism, the isoform bias identified is potentially of therapeutic relevance. Previous studies have extended analysis of biased signaling to naturally occurring mutant variants of the G protein–coupled calcium-sensing receptor, demonstrating significant changes in the signaling profile that, in part, account for their role in various endocrine diseases (Leach et al., 2015). These data demonstrated that even single amino acid changes result in different receptor conformations that give rise to biased signaling. Unsurprisingly, therefore, the more significant changes in amino acid sequence resulting from gene splicing for the H_3R readily yield change in biased signaling profile. Nevertheless, we believe that this is the first example of differential signaling mediated by splice variants of the same G protein–coupled receptor. Given that these histamine receptor isoforms have subtly different expression profiles in the brain, further experiments are required to determine whether the observed bias links to central nervous system diseases—for example, those in which both GSK3β and the histamine H_3 receptor have been implicated, such as schizophrenia and Alzheimer's disease

(Hooper et al., 2008; DaRocha-Souto et al., 2012; Cole, 2013). Studies in rat tissue have suggested that the well described autoreceptor function of the histamine H_3 receptor to control histamine release may be mediated primarily by a truncated isoform (Gbahou et al., 2012), implying that the hH_3R_{365} isoform could play this role in humans. If this were the case, the differential activation of downstream effector systems may have evolved to be an autoreceptor-specific mechanism; the data herein indicate that it might be possible to design drugs that selectively target individual H_3R isoforms. This also may have implications for other receptors for which known variants exist and biased agonism or allosteric modulation has been previously documented, e.g., dopamine D_2 receptors (Shonberg et al., 2013; Weichert et al., 2015) and metabotropic glutamate 5 receptors (Noetzel et al., 2013; Rook et al., 2015).

In summary, a cross-wise evaluation of five agonists at multiple signaling pathways downstream of the two main histamine H_3 receptor isoforms clearly identified significant ligand-directed biased signaling, most notably for proxyfan, corroborating previous studies describing this compound as a protean agonist. However, even more striking was the identification of isoform bias in our study, the first quantitative evidence, to our knowledge, of this phenomenon in the GPCR field. Although the etiology of the differential bias is not yet clear, it may help guide future discovery efforts targeting the histamine H_3 receptor.

Authorship Contributions

Participated in research design: Riddy, Cook, Mannoury la Cour, Mocaer, Summers, Sexton, Christopoulos, Langmead.

Conducted experiments: Riddy, Cook, Diepenhorst, Bosnyak.

Contributed new reagents or analytic tools: Brady.

Performed data analysis: Riddy, Cook, Diepenhorst, Bosnyak, Langmead.

Wrote or contributed to the writing of the manuscript: Riddy, Summers, Charman, Sexton, Christopoulos, Langmead.

References

Arrang J-M, Morisset S, and Gbahou F (2007) Constitutive activity of the histamine H3 receptor. *Trends Pharmacol Sci* **28**:350–357.

Barbier AJ, Aluisio L, Lord B, Qu Y, Wilson SJ, Boggs JD, Bonaventure P, Miller K, Fraser I, Dvorak L, et al. (2007) Pharmacological characterization of JNJ-28583867, a histamine H(3) receptor antagonist and serotonin reuptake inhibitor. *Eur J Pharmacol* **576**:43–54.

Barbier AJ, Berridge C, Dugovic C, Laposky AD, Wilson SJ, Boggs J, Aluisio L, Lord B, Mazur C, Pudiak CM, et al. (2004) Acute wake-promoting actions of JNJ-5207852, a novel, diamine-based H3 antagonist. *Br J Pharmacol* **143**:649–661.

Berchiche YA and Sakmar TP (2016) CXC Chemokine Receptor 3 Alternative Splice Variants Selectively Activate Different Signaling Pathways. *Mol Pharmacol* **90**: 483–495.

Berlin M, Boyce CW, and Ruiz M de L (2011) Histamine H3 receptor as a drug discovery target. *J Med Chem* **54**:26–53.

Bhowmik M, Khanam R, and Vohora D (2012) Histamine H3 receptor antagonists in relation to epilepsy and neurodegeneration: a systemic consideration of recent progress and perspectives. *Br J Pharmacol* **167**:1398–1414.

Bitner RS, Markosyan S, Nikkel AL, and Brioni JD (2011) In-vivo histamine H3 receptor antagonism activates cellular signaling suggestive of symptomatic and disease modifying efficacy in Alzheimer's disease. *Neuropharmacology* **60**:460–466.

Bongers G, Krueger KM, Miller TR, Baranowski JL, Estvander BR, Witte DG, Strakhova MI, van Meer P, Bakker RA, Cowart MD, et al. (2007) An 80-amino acid deletion in the third intracellular loop of a naturally occurring human histamine H3 isoform confers pharmacological differences and constitutive activity. *J Pharmacol Exp Ther* **323**:888–898.

Christopoulos A (1998) Assessing the distribution of parameters in models of ligand-receptor interaction: to log or not to log. *Trends Pharmacol Sci* **19**:351–357.

Cogé F, Guénin SP, Audinot V, Renouard-Try A, Beauverger P, Macia C, Ouvry C, Nagel N, Rique H, Boutin JA, et al. (2001) Genomic organization and characterization of splice variants of the human histamine H3 receptor. *Biochem J* **355**: 279–288.

Cole AR (2013) Glycogen synthase kinase 3 substrates in mood disorders and schizophrenia. *FEBS J* **280**:5213–5227.

Copeland R A (2016). The drug-target residence time model: a 10-year retrospective. *Nat Rev Drug Discov* **15**:87–95.

DaRocha-Souto B, Coma M, Pérez-Nievas BG, Scotton TC, Siao M, Sánchez-Ferrer P, Hashimoto T, Fan Z, Hudry E, Barroeta I, et al. (2012) Activation of glycogen synthase kinase-3 beta mediates β-amyloid induced neuritic damage in Alzheimer's disease. *Neurobiol Dis* **45**:425–437.

Dror RO, Mildorf TJ, Hilger D, Manglik A, Borhani DW, Arlow DH, Philippsen A, Villanueva N, Yang Z, Lerch MT, et al. (2015) SIGNAL TRANSDUCTION. Structural basis for nucleotide exchange in heterotrimeric G proteins. *Science* **348**: 1361–1365.

Esbenshade TA, Browman KE, Bitner RS, Strakhova M, Cowart MD, and Brioni JD (2008) The histamine H3 receptor: an attractive target for the treatment of cognitive disorders. *Br J Pharmacol* **154**:1166–1181.

Esbenshade TA, Krueger KM, Yao BB, Witte DG, Estvander BR, Baranowski JL, Miller TR, and Hancock AA (2006) Differences in pharmacological properties of histamine H(3) receptor agonists and antagonists revealed at two human H (3) receptor isoforms. *Inflamm Res* **55** (Suppl 1):S45–S46.

Gbahou F, Rouleau A, and Arrang J-M (2012) The histamine autoreceptor is a short isoform of the H_3 receptor. *Br J Pharmacol* **166**:1860–1871.

Gbahou F, Rouleau A, Morisset S, Parmentier R, Crochet S, Lin J-S, Ligneau X, Tardivel-Lacombe J, Stark H, Schunack W, et al. (2003) Protean agonism at histamine H3 receptors in vitro and in vivo. *Proc Natl Acad Sci USA* **100**: 11086–11091.

Gesty-Palmer D, Flannery P, Yuan L, Corsino L, Spurney R, Lefkowitz RJ, and Luttrell LM (2009) A beta-arrestin-biased agonist of the parathyroid hormone receptor (PTH1R) promotes bone formation independent of G protein activation. *Sci Transl Med* **1**:1ra1.

Giannoni P, Medhurst AD, Passani MB, Giovannini MG, Ballini C, Corte LD, and Blandina P (2010) Regional differential effects of the novel histamine H3 receptor antagonist 6-[(3-cyclobutyl-2,3,4,5-tetrahydro-1H-3-benzazepin-7-yl)oxy]-N-methyl-3-pyridinecarboxamide hydrochloride (GSK189254) on histamine release in the central nervous system of freely moving rats. *J Pharmacol Exp Ther* **332**: 164–172.

Hoffmann C, Castro M, Rinken A, Leurs R, Hill SJ, and Vischer HF (2015) Ligand Residence Time at G-protein-Coupled Receptors-Why We Should Take Our Time To Study It. *Mol Pharmacol* **88**:552–560.

Hooper C, Killick R, and Lovestone S (2008) The GSK3 hypothesis of Alzheimer's disease. *J Neurochem* **104**:1433–1439.

Huang C-C and Tesmer JJG (2011) Recognition in the face of diversity: interactions of heterotrimeric G proteins and G protein-coupled receptor (GPCR) kinases with activated GPCRs. *J Biol Chem* **286**:7715–7721.

Kenakin T (2011) Functional selectivity and biased receptor signaling. *J Pharmacol Exp Ther* **336**:296–302.

Kenakin T and Christopoulos A (2013) Signalling bias in new drug discovery: detection, quantification and therapeutic impact. *Nat Rev Drug Discov* **12**:205–216.

Kenakin T, Watson C, Muniz-Medina V, Christopoulos A, and Novick S (2012) A simple method for quantifying functional selectivity and agonist bias. *ACS Chem Neurosci* **3**:193–203.

Klein Herenbrink C, Sykes DA, Donthamsetti P, Canals M, Coudrat T, Shonberg J, Scammells PJ, Capuano B, Sexton PM, Charlton SJ, et al. (2016) The role of kinetic context in apparent biased agonism at GPCRs. *Nat Commun* **7**:10842.

Koole C, Savage EE, Christopoulos A, Miller LJ, Sexton PM, and Wootten D (2013) Minireview: Signal bias, allosterism, and polymorphic variation at the GLP-1R: implications for drug discovery. *Mol Endocrinol* **27**:1234–1244.

Krueger KM, Witte DG, Ireland-Denny L, Miller TR, Baranowski JL, Buckner S, Milicic I, Esbenshade TA, and Hancock AA (2005) G protein-dependent pharmacology of histamine H3 receptor ligands: evidence for heterogeneous active state receptor conformations. *J Pharmacol Exp Ther* **314**:271–281.

Kruse AC, Hu J, Pan AC, Arlow DH, Rosenbaum DM, Rosemond E, Green HF, Liu T, Chae PS, Dror RO, et al. (2012) Structure and dynamics of the M3 muscarinic acetylcholine receptor. *Nature* **482**:552–556.

Leach K, Conigrave AD, Sexton PM, and Christopoulos A (2015) Towards tissue-specific pharmacology: insights from the calcium-sensing receptor as a paradigm for GPCR (patho)physiological bias. *Trends Pharmacol Sci* **36**:215–225.

Leurs R, Bakker RA, Timmerman H, and de Esch IJP (2005) The histamine H3 receptor: from gene cloning to H3 receptor drugs. *Nat Rev Drug Discov* **4**:107–120.

Ligneau X, Perrin D, Landais L, Camelin JC, Calmels TPG, Berrebi-Bertrand I, Lecomte JM, Parmentier R, Anaclet C, Lin JS, et al. (2007) BF2.649 [1-3-[3-(4-Chlorophenyl)propoxy]propylpiperidine, hydrochloride], a nonimidazole inverse agonist/antagonist at the human histamine H3 receptor: Preclinical pharmacology. *J Pharmacol Exp Ther* **320**:365–375.

Liu JJ, Horst R, Katritch V, Stevens RC, and Wüthrich K (2012) Biased signaling pathways in β2-adrenergic receptor characterized by 19F-NMR. *Science* **335**: 1106–1110.

Medhurst AD, Atkins AR, Beresford IJ, Brackenborough K, Briggs MA, Calver AR, Cilia J, Cluderay JE, Crook B, Davis JB, et al. (2007) GSK189254, a novel H3 receptor antagonist that binds to histamine H3 receptors in Alzheimer's disease brain and improves cognitive performance in preclinical models. *J Pharmacol Exp Ther* **321**:1032–1045.

Morisset S, Rouleau A, Ligneau X, Gbahou F, Tardivel-Lacombe J, Stark H, Schunack W, Ganellin CR, Schwartz JC, and Arrang J-M (2000) High constitutive activity of native H3 receptors regulates histamine neurons in brain. *Nature* **408**:860–864.

Nijmeijer S, Vischer HF, Sirci F, Schultes S, Engelhardt H, de Graaf C, Rosethorne EM, Charlton SJ, and Leurs R (2013) Detailed analysis of biased histamine H_4 receptor signalling by JNJ 7777120 analogues. *Br J Pharmacol* **170**:78–88.

Noetzel MJ, Gregory KJ, Vinson PN, Manka JT, Stauffer SR, Lindsley CW, Niswender CM, Xiang Z, and Conn PJ (2013) A novel metabotropic glutamate receptor 5 positive allosteric modulator acts at a unique site and confers stimulus bias to mGlu5 signaling. *Mol Pharmacol* **83**:835–847.

O'Dowd BF, Hnatowich M, Regan JW, Leader WM, Caron MG, and Lefkowitz RJ (1988) Site-directed mutagenesis of the cytoplasmic domains of the human beta 2-adrenergic receptor. Localization of regions involved in G protein-receptor coupling. *J Biol Chem* **263**:15985–15992.

Pedregosa F, Varoquaux G, Gramfort A, Michel C, Thirion B, Grisel O, Blondel M, Prettenhofer P, Weiss R, Dubourg V, et al. (2011) Scikit-learn: Machine learning in Python. *J Mach Learn Res* **12**:2825–2830.

Pillot C, Heron A, Cochois V, Tardivel-Lacombe J, Ligneau X, Schwartz JC, and Arrang JM (2002) A detailed mapping of the histamine H(3) receptor and its gene transcripts in rat brain. *Neuroscience* **114**:173–193.

Riddy DM, Valant C, Rueda P, Charman WN, Sexton PM, Summers RJ, Christopoulos A, and Langmead CJ (2015) Label-Free Kinetics: Exploiting Functional Hemi-Equilibrium to Derive Rate Constants for Muscarinic Receptor Antagonists. *Mol Pharmacol* **88**:779–790.

Rook JM, Xiang Z, Lv X, Ghoshal A, Dickerson JW, Bridges TM, Johnson KA, Foster DJ, Gregory KJ, Vinson PN, et al. (2015) Biased mGlu5-Positive Allosteric Modulators Provide In Vivo Efficacy without Potentiating mGlu5 Modulation of NMDAR Currents. *Neuron* **86**:1029–1040.

Sahlholm K, Nilsson J, Marcellino D, Fuxe K, and Århem P (2012) Voltage sensitivities and deactivation kinetics of histamine H_3 and H_4 receptors. *Biochim Biophys Acta* **1818**:3081–3089.

Sato M, Horinouchi T, Hutchinson DS, Evans BA, and Summers RJ (2007) Ligand-directed signaling at the beta3-adrenoceptor produced by 3-(2-Ethylphenoxy)-1-[(1, S)-1,2,3,4-tetrahydronapth-1-ylamino]-2S-2-propanol oxalate (SR59230A) relative to receptor agonists. *Mol Pharmacol* **72**:1359–1368.

Schnell D, Burleigh K, Trick J, and Seifert R (2010) No evidence for functional selectivity of proxyfan at the human histamine H3 receptor coupled to defined Gi/Go protein heterotrimers. *J Pharmacol Exp Ther* **332**:996–1005.

Schwartz J-C (2011) The histamine H3 receptor: from discovery to clinical trials with pitolisant. *Br J Pharmacol* **163**:713–721.

Scott Bitner R (2012) Cyclic AMP response element-binding protein (CREB) phosphorylation: a mechanistic marker in the development of memory enhancing Alzheimer's disease therapeutics. *Biochem Pharmacol* **83**:705–714.

Shonberg J, Herenbrink CK, López L, Christopoulos A, Scammells PJ, Capuano B, and Lane JR (2013) A structure-activity analysis of biased agonism at the dopamine D2 receptor. *J Med Chem* **56**:9199–9221.

Stark H, Purand K, Hüls A, Ligneau X, Garbarg M, Schwartz JC, and Schunack W (1996) [125I]iodoproxyfan and related compounds: a reversible radioligand and novel classes of antagonists with high affinity and selectivity for the histamine H3 receptor. *J Med Chem* **39**:1220–1226.

Sykes DA, Dowling MR, and Charlton SJ (2009) Exploring the mechanism of agonist efficacy: a relationship between efficacy and agonist dissociation rate at the muscarinic M3 receptor. *Mol Pharmacol* **76**:543–551.

Thompson GL, Lane JR, Coudrat T, Sexton PM, Christopoulos A, and Canals M (2015) Biased Agonism of Endogenous Opioid Peptides at the μ-Opioid Receptor. *Mol Pharmacol* **88**:335–346.

Tiligada E, Zampeli E, Sander K, and Stark H (2009) Histamine H3 and H4 receptors as novel drug targets. *Expert Opin Investig Drugs* **18**:1519–1531.

Valant C, May LT, Aurelio L, Chuo CH, White PJ, Baltos J-A, Sexton PM, Scammells PJ, and Christopoulos A (2014) Separation of on-target efficacy from adverse effects through rational design of a bitopic adenosine receptor agonist. *Proc Natl Acad Sci USA* **111**:4614–4619.

Ward RJ, Alvarez-Curto E, and Milligan G (2011) Using the Flp-In™ T-Rex™ system to regulate GPCR expression. *Methods Mol Biol* **746**:21–37.

Weichert D, Banerjee A, Hiller C, Kling RC, Hübner H, and Gmeiner P (2015) Molecular determinants of biased agonism at the dopamine D_2 receptor. *J Med Chem* **58**:2703–2717.

Wellendorph P, Goodman MW, Burstein ES, Nash NR, Brann MR, and Weiner DM (2002) Molecular cloning and pharmacology of functionally distinct isoforms of the human histamine H(3) receptor. *Neuropharmacology* **42**:929–940.

Wold S, Esbensen K, and Geladi P (1987) Principal component analysis. *Chemom Intell Lab Syst* **2**:37–52.

Address correspondence to: Dr. Christopher J. Langmead, Drug Discovery Biology, Monash Institute of Pharmaceutical Sciences, Monash University, 381 Royal Parade, Parkville, VIC, 3052, Australia. E-mail: chris.langmead@monash.edu